2018 Annual American Control Conference (ACC)
June 27–29, 2018. Wisconsin Center, Milwaukee, USA

Data-Driven Feedforward Learning using Non-Causal Rational Basis Functions: Application to an Industrial Flatbed Printer

Lennart Blanken, Goksan Isil, Sjirk Koekebakker, Tom Oomen

Abstract— **Data-driven feedforward learning enables high performance for industrial motion systems based on measured data from previous motion tasks. The key aspect herein is the chosen feedforward parametrization, which should parsimoniously model the inverse system. At present, high performance comes at the cost of parametrizations that are nonlinear in the parameters and consequences thereof. A linear parametrization is proposed that enables parsimonious modeling of inverse systems for feedforward through the use of non-causal rational orthonormal basis functions. The benefits of the proposed parametrization are experimentally demonstrated on an industrial printer, including pre-actuation and cyclic pole repetition.**

I. INTRODUCTION

Feedforward control is widely used in control systems, since it can effectively compensate for known disturbances before these affect the system. For servo systems, the main performance improvement is typically achieved by compensating for the reference signal, which can be different for various tracking tasks. Successful feedforward control approaches include inverse model-based feedforward [1], [2] and iterative learning control (ILC) [3], [4].

On the one hand, inverse model-based feedforward generally results in moderate performance for a wide class of motion tasks. A parametric model of the inverse system is used, obtained (i) by inverting an identified model of the forward system, or (ii) by direct identification of the inverse system, see, e.g., [5]. Yet, the achievable performance is highly dependent on the accuracy of the model inversion, and the 'quality' of the inverse model [6]: it should be capable to accurately compensate the excited dynamics between reference and error. Especially for lightly damped mechatronic systems such as the flatbed printer in Fig. 1, accurate models can be difficult and expensive to obtain due to, e.g., complex dynamics [7], [8] and numerical issues [9].

On the other hand, ILC enables extremely high performance for a single, specific task. By learning from measured data from previous tasks, the need for an accurate model of the system is avoided. However, extrapolation of the learned control signal to other tasks in general leads to a significant performance deterioration, see, e.g., [10], [11], [12].

Recent developments in data-driven feedforward control aim to achieve (i) high performance for varying tasks, (ii) without requiring an accurate system model. This is enabled through a parametrization for the inverse system, whose parameters are iteratively estimated based on data from previous tasks. The key difficulty is choosing a suitable model structure and complexity. For performance, the parametrization should be parsimonious to avoid variance-induced errors, yet be capable to compensate reference-induced errors.

Model structures that are linear in the parameters are attractive due to the associated convex optimization problem. In [13], [14], [15], a linear combination of polynomial basis functions is used. However, the tracking performance is limited due to the polynomial nature of the feedforward controller. Especially for lightly damped systems, high order polynomials are required to accurately describe the inverse system, which are susceptible to noise acting on the system.

In [12], [16], [17], a rational model structure is proposed in combination with polynomial basis functions, which has shown to significantly improve performance using a small number of parameters. However, since the associated optimization problem becomes non-convex, nonlinear optimization algorithms are required for which, in general, convergence to the global minimum cannot be guaranteed.

Although important progress has been made towards improving performance in feedforward control, at present high performance comes at the cost of (i) non-convex optimization, or (ii) inflexibility to varying reference tasks. The aim of this paper is to propose a suitable inverse-model parametrization for data-driven feedforward control, which (i) is linear in the parameters, (ii) requires a small number of parameters, and (iii) enables infinite pre-actuation and post-actuation. The proposed approach is based on the use of non-causal rational orthonormal basis functions (OBFs). Whereas the use of *causal* OBFs has received significant attention in the field of system identification to model systems in $\mathcal{H}_2$, see, e.g., [18], [19], [20], here the use of *non-causal* functions is advocated to model inverse systems in $\mathcal{L}_2$. In particular, through stable inversion techniques [21], [22], the functions enable infinite pre-actuation for high performance feedforward control. The contributions of this paper are:

- Development of a parsimonious parametrization for inverse systems that is linear in the parameters, and enables non-causal feedforward control (Section III);
- Experimental validation of the proposed parametrization for feedforward learning on an industrial flatbed printer, demonstrating the benefits of using non-causal rational basis functions, including pre-actuation (Section IV).

The focus of this paper is on the modeling aspect and experimental validation, while details on the used algorithm for data-driven learning in Section IV can be found in [23].

L. Blanken, G. Isil and T. Oomen are with the Eindhoven University of Technology, Department of Mechanical Engineering, Control Systems Technology Group, Eindhoven, The Netherlands. S. Koekebakker is with Océ Technologies B.V., Venlo, The Netherlands. Email: L.L.G.Blanken@tue.nl.
This work is supported by Océ Technologies, and is part of the research programme VIDI with project number 15698, which is (partly) financed by the Netherlands Organisation for Scientific Research (NWO).

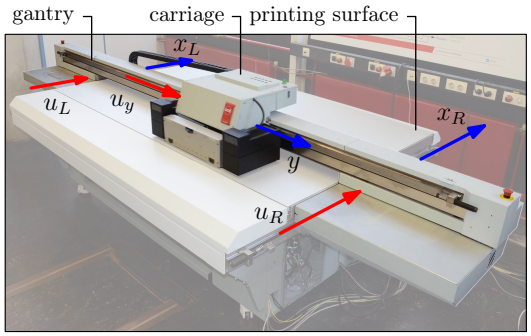

Fig. 1. Océ Arizona 550 GT flatbed printing system, with inputs indicated in red and outputs in blue. For experiments, the system P between non-collocated input u_L and output x_R is considered, which has NMP dynamics.

Notation: All systems are discrete-time, single-input single-output (SISO), and linear time-invariant. The complex indeterminate $z \in \mathbb{C}$ is omitted when this does not lead to any confusion. The following standard notation is used, see, e.g., [19]. Let $\mathbb{D}$ denote the open unit disk: $\{z, |z| < 1\}$, $\mathbb{E}$ the complement of the closed unit disk: $\{z, |z| > 1\}$, and $\mathbb{T}$ the unit circle: $\{z, |z| = 1\}$. $\mathcal{L}_2$ denotes the set of complex functions that are square integrable on $\mathbb{T}$, and the real rational subspace of $\mathcal{L}_2$ is denoted $\mathcal{RL}_2$. $\mathcal{H}_2$ denotes the set of complex functions that are square integrable on $\mathbb{T}$ and analytic for $|z| \geq 1$. The space $\mathcal{H}_{2-}$ denotes all functions in $\mathcal{H}_2$ that are zero at infinity, such as strictly proper systems, and $\mathcal{H}_{2-}^{\perp} = \mathcal{L}_2 \setminus \mathcal{H}_{2-}$. $\mathbb{R}[z^{-1}]$ denotes the polynomial ring in indeterminate z^{-1} with coefficients in $\mathbb{R}$, and $\mathbb{R}[z, z^{-1}]$ denotes the Laurent polynomial ring in indeterminate z with coefficients in $\mathbb{R}$. Contrary to regular polynomials, Laurent polynomials include both positive and negative exponents of the indeterminate. The space of all square summable sequences is denoted ℓ_2. For a vector $x \in \mathbb{R}^N$, the weighted two-norm is given by $\|x\|_W^2 = x^\top W x$ with $W \in \mathbb{R}^{N \times N}$. W is positive definite if $x^\top W x > 0$, $\forall x \neq 0$.

II. DATA-DRIVEN FEEDFORWARD CONTROL

A. Experimental Setup

The considered motion system is an Océ Arizona 550 GT, see Fig. 1. In contrast to standard consumer printers, the medium is fixed on the printing surface. The carriage, which contains the printheads, translates in y-direction along the gantry, which translates in x and rotates in R_z. The system is equipped with three current-driven brushless electrical motors to provide the required forces. The measurement system consists of three optical encoders, collocated with the actuators, yielding position measurements x_L, x_R and y. A stabilizing multivariable feedback controller is implemented. The system operates with sampling time 10^{-3} s.

B. Control Configuration

The input and output considered for control are the current u_L [A] to the actuator on the left side of the gantry, and the position x_R [m] on the right side of the gantry, respectively. By closing all feedback loops, a SISO equivalent system P is obtained, i.e. $P : u_L \to x_R$. Since all performed translations and rotations are small, the system is assumed linear.

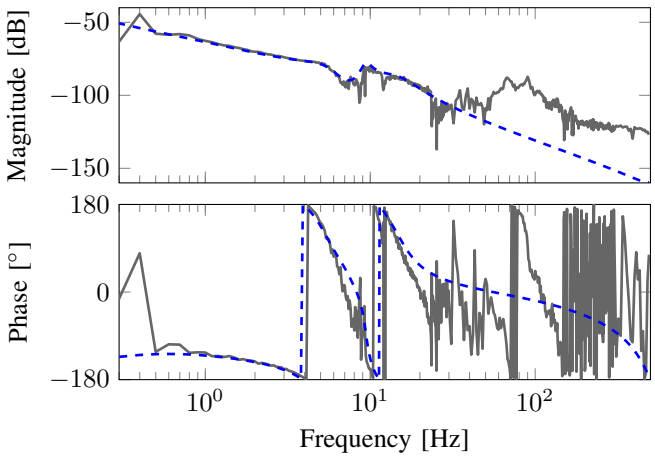

Fig. 2. Bode diagram of FRF measurement of P (——), and approximate model $\hat{P}$ (– –). The non-minimum phase dynamics can be observed around the anti-resonance around 7 Hz: the phase lag increases by 180 degrees.

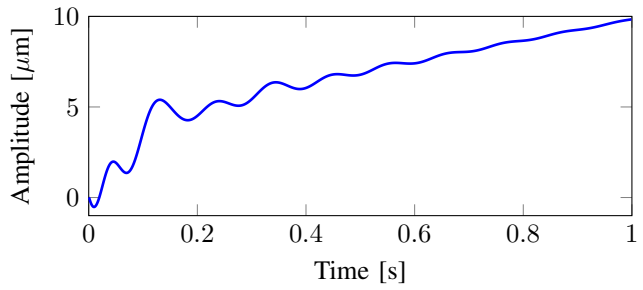

Fig. 3. Impulse response of model $\hat{P}$: due to its non-minimum phase dynamics, the system initially moves in negative direction.

An identified frequency response function of P is shown in Fig. 2. Interestingly, due to the non-collocated input/output pairing, the system exhibits non-minimum phase (NMP) dynamics. This can be observed from Fig. 2 by the Bode gain-phase relationship: around the anti-resonance at 7 Hz, the phase lag increases by 180 degrees. An approximate 10th order parametric model $\hat{P}$ is identified for control design in Section IV, containing three NMP zeros in $\mathbb{E}$, two of which can clearly be observed in Fig. 2 at 7 Hz. Its impulse response in Fig. 3 initially moves in the opposite direction, confirming the non-minimum phase dynamics.

The control configuration is schematically shown in Fig. 4. The plant $P(z)$ is described by the rational representation

$$P(z) = \frac{B_0(z)}{A_0(z)},$$

with $A_0(z), B_0(z) \in \mathbb{R}[z^{-1}]$. The control configuration consists of a given stabilizing feedback controller $C(z)$, and a feedforward controller $F(z)$. Let r denote the reference signal, y the output signal, and f the feedforward signal. The tracking error signal $e = r - y$ is given by

$$e(t) = S(q)\left(I - P(q)F(q)\right) r(t), \tag{1}$$

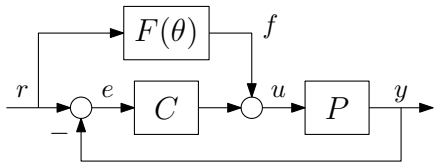

Fig. 4. Control configuration for feedforward learning.

with $S(z) = (I + P(z)C(z))^{-1}$. Perfect tracking, i.e., $e = 0$, for all $r \neq 0$ is achieved if $F(q) = P^{-1}(q)$. Next, a data-driven estimation approach for inversion-based feedforward is proposed, aiming to minimize (1).

C. Data-Driven Feedforward Learning

In data-driven feedforward learning, measured batches of data from previous tasks, denoted by index $j = 1, 2, \ldots$, are used to determine a fixed-structure controller. That is,

$$f_j = F(\theta_j)r,$$

with parameters $\theta \in \mathbb{R}^{n_\theta}$ and $F(\theta) \in \mathcal{F}$ with feedforward parametrization $\mathcal{F}$. Then, θ_{j+1} for the next task is determined based on a data-driven optimization problem, e.g.,

$$\hat{\theta}_{j+1} = \arg\min_{\theta} V(\theta), \tag{2}$$

where the data-based performance criterion $V(\theta)$ is typically of the following general form, see, e.g., [12], [13], [14], [23],

$$V(\theta_{j+1}) = \|e_{j+1}\|_{W_e} + \|f_{j+1}\|_{W_f} + \|f_{j+1} - f_j\|_{W_{\Delta f}}, \tag{3}$$

with weight matrices $W_e \succ 0$, $W_f, W_{\Delta f} \succeq 0$. W_f and $W_{\Delta f}$ are typically chosen as small as possible to minimize $\|e_{j+1}\|$, yet can be used to balance robustness and convergence properties of the learning algorithm [24]. Details on data-based algorithms can be found in, e.g., [12], [13], [14], [23].

A key aspect to effectively reduce (1) for all r, apart from the chosen optimization algorithm, is to select an appropriate feedforward parametrization. On the one hand, $F(\theta)$ should capture the behavior of P^{-1} at frequencies where r has dominant energy. To see this, represent (1) in the frequency domain: $E(\omega) = S(e^{i\omega})\left(I - P(e^{i\omega})F(e^{i\omega})\right)R(\omega)$. On the other hand, the model complexity should not be too high, since this may lead to large variance errors due to overparametrization, which can result in inflexibility to varying r.

D. Feedforward Parametrization

An attractive property of model structures is linearity in the parameters, since this enables convex optimization in (2).

Definition 1 (Linear feedforward parametrization)**.** *The feedforward controller $F(\theta)$ is parameterized as*

$$\mathcal{F}_{lin} = \left\{F(z,\theta) = \theta\Psi(z) = \sum_{k=1}^{n_\theta} \theta_k \psi_k(z)\right\} \tag{4}$$

with basis functions $\Psi(z) = [\psi_i(z), \ldots, \psi_{n_\theta(z)}]^\top$.

Crucially, for $\mathcal{F}_{\text{lin}}$ and a quadratic cost function $V(\theta)$, there exists an analytic solution for $\hat{\theta}$ in (2). This is in contrast with the rational feedforward structure used in [12], [16].

The basis functions are often chosen as Laurent polynomials $\psi_k(z) \in \mathbb{R}[z, z^{-1}]$, see, e.g., [13], [14], [15]. This generalizes the widely used finite impulse response (FIR) models in system identification [25], yet crucially allows for the use of preview. However, due to the polynomial nature of the functions, a high number of parameters might be required to accurately model P^{-1}, especially for rational systems with slow, lightly damped dynamics and fast sampling rates.

E. Contributions

The main contributions of this paper are the following.

C1. A parametrization is proposed to parsimoniously model inverse systems for feedforward control, that
- is linear in the parameters, hence enabling convex data-based feedforward learning in (2);
- uses a small number of parameters;
- and enables the use of infinite pre-actuation.

C2. Experimental validation of C1 on the industrial printing system in Fig. 1, demonstrating enhanced performance compared to non-causal FIR parametrizations.

III. NON-CAUSAL RATIONAL BASIS FUNCTIONS FOR FEEDFORWARD CONTROL

In this section, the use of non-causal OBFs is advocated to model inverse systems in $\mathcal{L}_2$. This is in contrast with the field of system identification, which generally focuses on modeling stable, causal systems in $\mathcal{H}_2$, see, e.g., [18], [19], [20]. Crucially, these functions enable (i) convex optimization, (ii) parsimonious modeling, and (ii) non-causal control.

In Subsection III-B, a construction procedure is presented for non-causal orthonormal basis functions. The orthonormality is with respect to standard inner product on $\mathcal{L}_2$:

$$\frac{1}{2\pi}\int_{-\pi}^{\pi} \psi_k(e^{i\omega})\psi_l(e^{-i\omega})d\omega = \begin{cases} 1 & \text{if } k = l, \\ 0 & \text{if } k \neq l. \end{cases}$$

A. Motivation

The proposed approach is motivated by the following duality of interpretation. If $P(z)$ has NMP zeros on $\mathbb{E}$, $P^{-1}(z)$ may be interpreted as an unbounded and causal operator on $\mathcal{L}_2$. In contrast, here P^{-1} is interpreted as a bounded and non-causal operator on $\mathcal{L}_2$ [26, Section 1.5]. Using the bilateral Z-transform, $P^{-1} \in \mathcal{RL}_2$ can be expressed as

$$P^{-1}(z) = \sum_{k=-\infty}^{\infty} p_k z^{-k}, \tag{5}$$

with $\{p_k\} \in \ell_2(-\infty, \infty)$ the sequence of Markov parameters. The impulse response $\{p_k\}$ arises from solving the underlying difference equation also for negative time. Crucially, this response is non-causal and infinitely long.

Hence, to accurately approximate (5) using a small number of parameters, it naturally makes sense to choose basis functions $\psi_k(z) \in \mathcal{RL}_2$, i.e., non-causal rational basis functions. That is, $F(z)$ is designed as the following finite expansion, see Definition 1, with infinite impulse response:

$$F(z) = \sum_{k=1}^{n_\theta} \theta_k \psi_k(z) = \sum_{k=-\infty}^{\infty} f_k z^{-k}.$$

B. Construction of Non-Causal Rational Basis Functions

The key aspect in constructing non-causal rational basis functions is specifying the fixed poles. Indeed, FIR basis functions have poles at $z = 0$, which is why many parameters are required to accurately approximate rational systems with lightly damped poles. Here, the poles are chosen in $\mathbb{D} \cup \mathbb{E}$.

The considered OBFs are defined by sequences $\xi_s = \{\xi_{s,k}\}_{k=1,2,\ldots}$ and $\xi_u = \{\xi_{u,k}\}_{k=1,2,\ldots}$, with $\xi_{s,k}, \xi_{u,k} \in \mathbb{D}$:

$$\psi_{s,k}(z) = \frac{\sqrt{1-|\xi_{s,k}|^2}}{z-\xi_{s,k}}\phi_k(z,\xi_s), \tag{6}$$

$$\psi_{u,k}(z) = \frac{\sqrt{1-|\xi_{u,k}|^2}}{1-\overline{\xi_{u,k}}z}\phi'_k(z,\xi_u), \tag{7}$$

where the all-pass transfer functions ϕ_k, ϕ'_k are defined by

$$\phi_k(z,\xi) = \begin{cases} 1 & \text{if } k = 1, \\ \prod_{m=1}^{k-1} \frac{1-\overline{\xi_m}z}{z-\xi_m} & \text{if } k > 1. \end{cases}$$

$$\phi'_k(z,\xi) = \begin{cases} 1 & \text{if } k = 1, \\ \prod_{m=1}^{k-1} \frac{z-\xi_m}{1-\overline{\xi_m}z} & \text{if } k > 1. \end{cases}$$

The sequence $\{\psi_{s,k}\}_{k>0} \in \mathcal{H}_{2-}$ forms the well-known Takenaka-Malmquist functions, and consists of strictly causal functions. The set $\{\psi_{u,k}\}_{k>0} \in \mathcal{H}_{2-}^{\perp}$ contains anti-causal functions and direct feedthrough terms, e.g., select $\xi_{u,1} = 0$. Indeed, note that the poles of the anti-causal $\psi_{u,k}$ and ϕ'_k, which is the reciprocal of ϕ_k, are located at $\{1/\overline{\xi_{u,k}}\} \subseteq \mathbb{E}$. When complex conjugated pole pairs are used, (6) and (7) must be adapted through a unitary transformation to obtain real-valued basis functions, see, e.g., [18], [27]. Together, (6) and (7) form the basis functions to be used:

$$\Psi(z) = [\psi_{s,1}(z), \psi_{s,2}(z), \ldots, \psi_{u,1}(z), \psi_{u,2}(z), \ldots]^\top.$$

As a guideline, $\{\xi_{s,k}\}$ and $\{\frac{1}{\xi_{u,k}}\}$ should be chosen as close as possible to what are believed the true poles of P^{-1}, see, e.g., [19, Chapter 11], and consider the following.

- The linear span of the basis functions $\Psi(z)$ is complete in $\mathcal{L}_p$, $1 < p < \infty$, if and only if $\sum_{k=1}^{\infty} 1 - |\xi_{s,k}| = \infty$ and $\sum_{k=1}^{\infty} 1 - |\xi_{u,k}| = \infty$. These mild conditions on the pole locations imply that any such orthonormal basis can arbitrarily well model any system in $\mathcal{L}_p$ [18], [27].
- Using a finite number of basis functions, the under-modeling error $|P^{-1}(e^{i\omega}) - F(e^{i\omega}, \theta^*)|$ can be upper bounded, see, e.g., [28, Theorem VI.1], which can be appropriately extended for systems in $\mathcal{L}_2$. $F(z, \theta^*)$ denotes the best approximation of $P^{-1}(z)$ in $\mathcal{L}_2$ sense. Importantly, the bound decreases with the Euclidean distance between ξ and the true poles of P^{-1}.

C. Cyclic Repetition of Poles

Given a finite and approximate set of poles, the approximation error can be reduced by cyclically repeating the poles, i.e., $\xi_{s,k+n} = \xi_{s,k}$ and $\xi_{u,k+n} = \xi_{u,k}$. In view of feedforward, this potentially improves tracking performance. The repeated basis is generated from the original basis by multiplications with all-pass functions ϕ_k, ϕ'_k, and hence differs only in phase. The benefits are illustrated next.

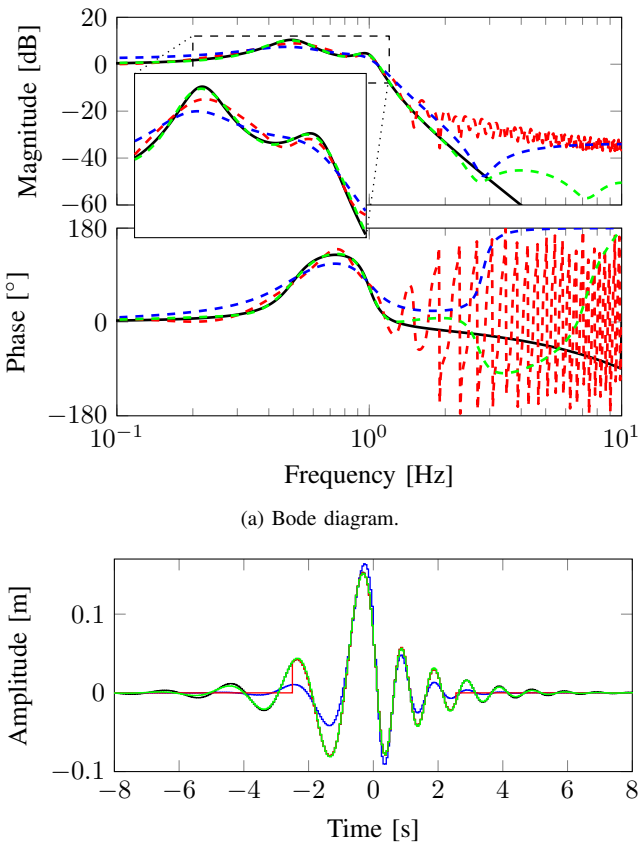

(a) Bode diagram.

(b) Impulse responses.

Fig. 5. Simulation example: Bode diagram (top) and non-causal impulse responses (bottom) of true system $G(z)$ (—), 100^{th} order FIR model (—), and 4^{th} (—) and 12^{th} (—) order models using rational basis functions.

Example 1 (Benefits of non-causal rational OBFs)**.** *Consider the continuous-time system*

$$G(s) = \prod_{i=1}^{2} \frac{\omega_i^2}{s^2 + 2\zeta_i\omega_i s + \omega_i^2},$$

where the first mode with natural frequency $\omega_1 = 1$ [Hz] and damping ratio $\zeta_1 = 0.1$ yields a complex pair of poles in $\mathbb{D}$, while the second mode with negative natural frequency $\omega_2 = -0.5$ [Hz] and $\zeta_2 = 0.2$ gives a complex pair of poles in $\mathbb{E}$. A discrete-time system $G(z) \in \mathcal{RL}_2$ is obtained using zero-order-hold with sampling time $T_s = 0.02$ [s].

Three models of $G(z)$ are estimated: a 100^{th} order FIR model with 50 anti-causal and 50 causal terms, and 4^{th} and 12^{th} order rational models with basis functions according to (6), (7). The poles $\{\xi_s\}$ and $\{\xi_u\}$ are chosen corresponding to the true poles of $G(z)$, except the damping ratios are chosen 2 times higher. For the 12^{th} order model, these poles are repeated three times. The parameters are obtained by minimizing $\int_{-\pi}^{\pi} |G(e^{i\omega}) - \theta\Psi(e^{i\omega})|^2 d\omega$. The results are shown in Fig. 5, and the following observations are made.

- *For the FIR model, a substantial error remains. In time-domain, this can be seen from the truncated response.*
- *By the rational OBFs and pole repetitions, the modeling error is significantly reduced using only 12 parameters.*

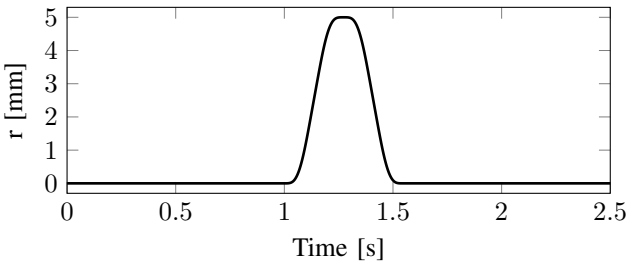

Fig. 6. Reference signal for experiments.

D. Design Procedure

In this section, a parametrization is proposed to efficiently model inverse systems for feedforward control, which uses a small number of parameters and enables the use of non-causal control actions. Next, a design procedure is presented for data-driven feedforward learning based on this result.

Procedure 1. Design procedure for data-driven feedforward learning using non-causal rational basis functions

1. Choose a finite set of poles in $\mathbb{D} \cup \mathbb{E}$ approximating those of P^{-1}, e.g., based on FRF measurements.
2. Construct a set of non-causal basis functions $\psi_k \in \mathcal{L}_2$ using (6), (7) for the feedforward parametrization (4).
3. Data-driven learning of θ, see, e.g., [13], [14], [23].
4. If the achieved performance is unsatisfactory, return to
   - step 1 and add or update fixed pole locations,
   - or, step 2 and add set of basis functions through cyclic repetition of same poles, see Subsection III-C.

IV. EXPERIMENTAL VALIDATION ON INDUSTRIAL FLATBED PRINTER

In this section, the proposed use of non-causal rational basis functions for data-driven feedforward control is experimentally validated on the setup in Fig. 1. The parameters are iteratively tuned using the ILC-based approach in [23] with criterion (3). The experimental contributions are:

- The tracking performance using OBFs is compared to FIR basis functions, including non-causal control usage.
- The performance benefits of cyclically repeating the basis poles are demonstrated.

For the iterative learning, 10 finite time tasks are performed with reference signal depicted in Fig. 6. The poles of the rational basis functions are chosen equal to the zeros of model $\hat{P}$, see Fig. 2, which are expected to coarsely approximate the true poles of P^{-1}, and are given by

$$\{\psi_{s,k}\} = \{0.9039, 0.9853, 0.9854 \pm 0.0457i, 0.9988\}, \quad (8)$$

$$\{\psi_{u,k}\} = \left\{0, \tfrac{1}{1.008 \pm 0.0477i}, \tfrac{1}{1.078}\right\}. \quad (9)$$

Here, $\psi_{u,1} = 0$ generates a feedthrough term. To compare the results based on different pole locations, the same number of causal and anti-causal FIR basis functions is generated, i.e., $\psi_k = z^{-k}$, with $k \in [-3, 6]$. All parameters are initialized as $\theta = 0$, i.e., only feedback is active in task $j = 1$.

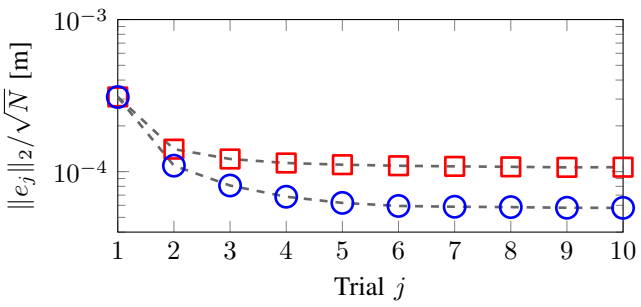

Fig. 7. Experimental results: feedforward learning using ILC. After 10 trials, 45% increased tracking performance is achieved using non-causal rational basis functions (—○—) compared to FIR basis functions (—□—).

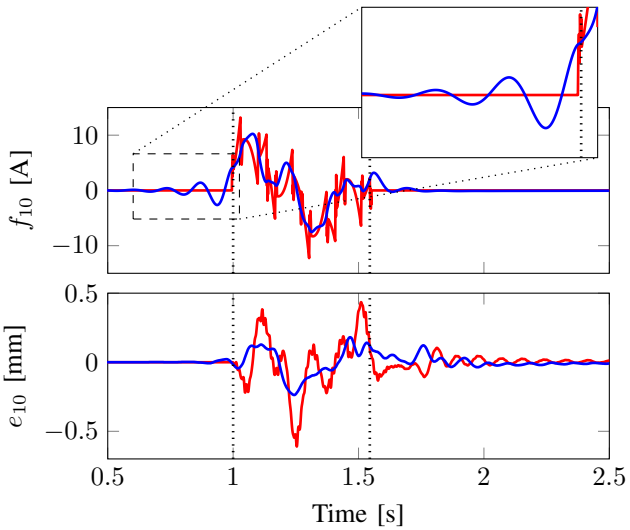

Fig. 8. Experimental results: the non-causal rational basis functions (——) with poles in $\mathbb{D}$ and $\mathbb{E}$ enable infinitely long pre-actuation and post-actuation. Compared to the (non-causal) FIR basis functions (——), which enable only a small and finite amount of preview, the error e_{10} is significantly reduced. The vertical dotted lines indicate the start and end of the motion task.

A. Influence of Selected Pole Locations

The benefits on tracking performance of choosing the basis poles in $\mathbb{D} \cup \mathbb{E}$, see (8) and (9), are compared to the poles $z = 0$ of the FIR basis functions. The ILC weights are $W_e = 50I$, $W_f = 10^{-7}I$, and $W_{\Delta f} = 0$. The results are presented in Figures 7 and 8, and the following observations are made.

- Using the proposed non-causal rational basis functions, the tracking performance $\|e_{10}\|_2$ is improved by 45% compared to the FIR basis functions.
- The three anti-causal basis functions (7) with poles in $\mathbb{E}$ generate infinitely long pre-actuation to effectively compensate the non-minimum phase dynamics of P. The anti-causal FIR basis functions generate only a finite amount of preview, i.e., 3 discrete time steps.

B. Cyclic Repetition of Fixed Poles

Next, the benefits on tracking performance of cyclically repeating the basis poles are experimentally demonstrated. The sequences (8) and (9) are repeated once, hence 10 strictly causal and 8 non-causal basis functions are generated. W_e

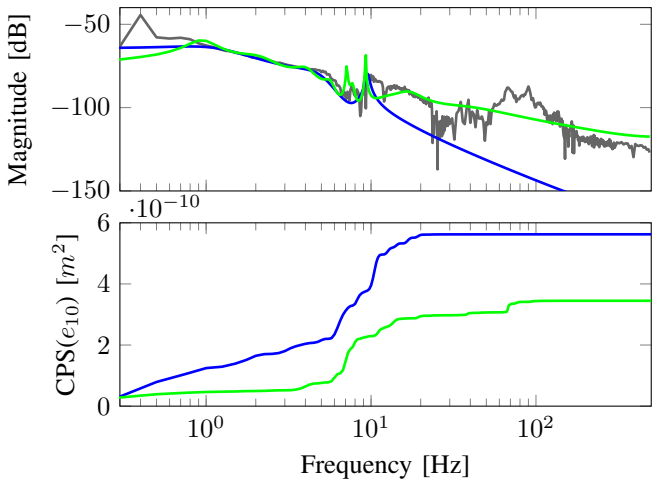

Fig. 9. Experimental results: benefits of cyclically repeating the poles. Bode magnitude diagram of P and $F^{-1}(\theta_{10})$ (top) and sample normalized cumulative power spectrum of e_{10} (bottom). By repeating the poles once (——) compared to the initial pole sets (8) and (9) (——), the power of e_{10} is reduced at frequencies where r has dominant power.

is increased to $W_e = 10^5 I$. The experimental results are presented in Fig. 9, and the following observations are made.

- By repeating the poles once, the tracking performance $\|e_{10}\|_2$ is decreased by 23%: the residual cumulative power at the Nyquist frequency (this is the RMS value $\|e_{10}\|_2^2$) is $(1 - 0.23)^2 \times 100\% = 60\%$. The main performance improvement is achieved below 20 Hz.
- At low frequencies, the inverse feedforward controllers $F(\theta)^{-1}$ reasonably approximate P. Since the excitation signal r has dominant power at low frequencies, F is not required to accurately approximate P^{-1} at higher frequencies, see also the power spectrum of e_{10}.

V. CONCLUSIONS

In this paper, a feedforward parametrization is presented for parsimonious modeling of inverse systems that is linear in the parameters. At present, compact model structures for high performance feedforward control come at the cost of nonlinear optimization problems at consequences thereof. The main contribution of this paper is the use of non-causal rational orthonormal basis functions in $\mathcal{L}_2$, that enable (i) convex optimization, (ii) compact modeling of inverse systems, and (iii) infinite pre-actuation. The benefits of the proposed approach are experimentally demonstrated on an industrial flatbed printer, including the benefits of infinite preview and cyclic pole repetition.

REFERENCES

[1] J. Butterworth, L. Pao, and D. Abramovitch, "Analysis and comparison of three discrete-time feedforward model-inverse control techniques for nonminimum-phase systems," *Mechatronics*, vol. 22, no. 5, pp. 577–587, 2012.

[2] G. M. Clayton, S. Tien, K. Leang, Q. Zou, and S. Devasia, "A review of feedforward control approaches in nanopositioning for high-speed SPM," *J. Dyn. Syst. Meas. Control*, vol. 131, no. 6, p. 061101, 2009.

[3] D. Bristow, M. Tharayil, and A. Alleyne, "A survey of iterative learning control," *IEEE Control Syst. Mag.*, vol. 26, no. 3, pp. 96–114, 2006.

[4] S. Gunnarsson and M. Norrlöf, "On the design of ILC algorithms using optimization," *Automatica*, vol. 37, no. 12, pp. 2011–2016, 2001.

[5] Y. Jung and M. Enqvist, "Estimating models of inverse systems," in *Proceedings of the 52nd IEEE Conference on Decision and Control*, Florence, Italy, 2013, pp. 7143–7148.

[6] S. Devasia, "Should model-based inverse inputs be used as feedforward under plant uncertainty?" *IEEE Trans. Automat. Contr.*, vol. 47, no. 11, pp. 1865–1871, 2002.

[7] M. Gevers, "Identification for control: From the early achievements to the revival of experiment design," *Eur. J. Control*, vol. 11, no. 4, pp. 335 – 352, 2005.

[8] H. Hjalmarsson, "System identification of complex and structured systems," *Eur. J. Control*, vol. 15, no. 3, pp. 275 – 310, 2009.

[9] R. van Herpen, O. Bosgra, and T. Oomen, "Bi-orthonormal polynomial basis function framework with applications in system identification," *IEEE Trans. Automat. Contr.*, vol. 61, no. 11, pp. 3285–3300, 2016.

[10] D. Hoelzle, A. Johnson, and A. Alleyne, "Bumpless transfer filter for exogenous feedforward signals," *IEEE Trans. Contr. Syst. Technol.*, vol. 22, no. 4, pp. 1581–1588, 2014.

[11] S. Mishra and M. Tomizuka, "Projection-based iterative learning control for wafer scanner systems," *IEEE/ASME Trans. Mechatron.*, vol. 14, no. 3, pp. 388–393, 2009.

[12] L. Blanken, F. Boeren, D. Bruijnen, and T. Oomen, "Batch-to-batch rational feedforward control: from iterative learning to identification approaches, with application to a wafer stage," *IEEE/ASME Trans. Mechatron.*, vol. 22, no. 2, pp. 826–837, 2017.

[13] F. Boeren, T. Oomen, and M. Steinbuch, "Iterative motion feedforward tuning: A data-driven approach based on instrumental variable identification," *Contr. Eng. Prac.*, vol. 37, pp. 11 – 19, 2015.

[14] J. Bolder, T. Oomen, S. Koekebakker, and M. Steinbuch, "Using iterative learning control with basis functions to compensate medium deformation in a wide-format inkjet printer," *Mechatronics*, vol. 24, no. 8, pp. 944 – 953, 2014.

[15] J. van de Wijdeven and O. Bosgra, "Using basis functions in iterative learning control: analysis and design theory," *Int. J. Control*, vol. 83, no. 4, pp. 661–675, 2010.

[16] J. Bolder, T. Oomen, and M. Steinbuch, "Rational basis functions in iterative learning control - with experimental verification on a motion system," *IEEE Trans. Contr. Syst. Technol.*, vol. 23, no. 2, pp. 722–729, 2015.

[17] F. Boeren, L. Blanken, D. Bruijnen, and T. Oomen, "Optimal estimation of rational feedforward control via instrumental variables: With application to a wafer stage," *Asian J. Control*, 2017, to appear.

[18] B. Ninness and F. Gustafsson, "A unifying construction of orthonormal bases for system identification," *IEEE Trans. Automat. Contr.*, vol. 42, no. 4, pp. 515–521, 1997.

[19] P. Heuberger, P. Van den Hof, and B. Wahlberg, *Modelling and Identification with rational orthogonal basis functions*. Springer-Verlag, London, UK, 2005.

[20] B. Wahlberg and P. Mäkilä, "On approximation of stable linear dynamical systems using Laguerre and Kautz functions," *Automatica*, vol. 32, no. 5, pp. 693 – 708, 1996.

[21] Q. Zou and S. Devasia, "Preview-based stable-inversion for output tracking of linear systems," *J. Dyn. Syst. Meas. Control*, vol. 121, no. 4, pp. 625–630, 1999.

[22] T. Sogo, "On the equivalence between stable inversion for nonminimum phase systems and reciprocal transfer functions defined by the two-sided Laplace transform," *Automatica*, vol. 46, no. 1, pp. 122 – 126, 2010.

[23] L. Blanken, G. Isil, S. Koekebakker, and T. Oomen, "Flexible ILC: Towards a convex approach for non-causal rational basis functions," *IFAC-PapersOnLine*, vol. 50, no. 1, pp. 12 107–12 112, 2017, IFAC 2017 World Congress, Toulouse, France.

[24] G. Pipeleers and K. L. Moore, "Reduced-order iterative learning control and a design strategy for optimal performance tradeoffs," *IEEE Trans. Automat. Contr.*, vol. 57, no. 9, pp. 2390–2395, 2012.

[25] L. Ljung, *System identification - Theory for the User*. Upper Saddle River, NY, USA: Prentice-Hall, 1999.

[26] G. Vinnicombe, *Uncertainty and Feedback: $\mathcal{H}_\infty$ loop-shaping and the ν-gap metric*. London, U.K.: Imperial College Press, 2001.

[27] H. Akçay, "Discrete-time system modelling in L_p with orthonormal basis functions," *Syst. Control Lett.*, vol. 39, no. 5, pp. 365–376, 2000.

[28] B. Ninness, H. Hjalmarsson, and F. Gustafsson, "The fundamental role of general orthonormal bases in system identification," *IEEE Trans. Automat. Contr.*, vol. 44, no. 7, pp. 1384–1406, 1999.